Calculation of Free Energy Profiles for Elementary Bimolecular Reactions by ab Initio Molecular Dynamics: Sampling Methods and Thermostat Considerations

Evan Kelly, Michael Seth, and Tom Ziegler*

Department of Chemistry, University of Calgary, 2500 University Drive, Calgary, Alberta, Canada T2N 1N4

Received: July 11, 2003; In Final Form: December 9, 2003

A study designed to refine the procedure for performing ab initio molecular dynamics calculations (AIMD) on chemical reactions is presented. Of key interest is the calculation of changes in free energy along the entire reaction path. Several simple elementary reactions are studied with the Car−Parrinello projector augmented-wave (CP−PAW) density-functional theory (DFT) methodology. The illustrative gas-phase bimolecular addition reactions are (i) a σ complexation of $BH_3 + H_2O \rightarrow H_2O{\cdot}BH_3$, (ii) the Diels−Alder reactions of butadiene with ethene, $C_4H_6 + C_2H_4 \rightarrow$ cyclohexene, 1,3-cyclopentadiene (CP) and ethene, CP $+ C_2H_4 \rightarrow$ norbornene, and the stereoselective reaction of 5-amino-CP with ethene, amino-CP $+ C_2H_4 \rightarrow$ amino-norbornene, (iii) the carbene cyclopropanation $Cl_2C + C_2H_4 \rightarrow Cl_2C_3H_4$, and (iv) the dimerization of ketene. These reactions were used to test both the slow-growth and point-wise thermodynamic integration (STI and PTI) methods of phase-space sampling as well as the Nosé−Hoover and Andersen thermostats. It is found that the PTI technique is potentially superior to the slow-growth method in terms of computational expense and is at least as accurate. The Nosé−Hoover thermostat appears to be inadequate for most of the reactions modeled here, whereas the stochastic Andersen thermostat affords more accurate results.

Introduction

In recent years, the range of application of ab initio molecular dynamics (AIMD) has expanded significantly with publications extending from small organic reactions to biochemical modeling.[1−7] An advantage of AIMD is that thermal effects, such as entropy, are included explicitly. In comparison, conventional quantum mechanical approaches add entropic effects through a frequency analysis, which can be computationally expensive. Such an analysis involves the harmonic approximation, which is not always valid.[8] This point is particularly important in studies of transition states (TS) where bonds are half-formed and therefore relatively weak. Examples are being found where finite temperature reaction paths significantly differ from statically calculated 0 K paths,[9] making dynamics a valuable tool in reaction analysis.

An important application of molecular simulations is the calculation of free energy paths and differences.[10] Many transformations of interest, including most chemical reactions, take place in time scales that are orders of magnitude longer than those accessible to dynamics simulations. To overcome this problem, a number of techniques have been developed, including thermodynamic perturbation[10,11] and thermodynamic integration.[12−15] In this work, we shall focus on the latter.

The calculation of free energy curves along a reaction path by thermodynamic integration (TI) in conjunction with molecular mechanics is fairly well established. AIMD can be applied to a number of problems for which molecular mechanics-based methods are unsuitable such as the making and breaking of covalent bonds. Although significant work has been carried out (for example, see refs 12−15, 77−80, and references therein), the potential of thermodynamic integration in combination with AIMD for these types of problems has not been fully explored. In the current investigation, we examine the performance of AIMD and thermodynamic integration as applied to a number of simple bimolecular addition reactions $A + B \rightarrow AB$. For reactions of this type, finite temperature effects (entropy) are substantial allowing the methods used to be thoroughly tested. Two aspects will be of special interest. The first is a comparison of slow-growth thermodynamic integration (STI) and point-wise thermodynamic integration (PTI) methods. The second will be the relative effectiveness of the Nosé and Andersen thermostats.

In an AIMD simulation the motion of the nuclei is governed by Newton's equations. Therefore, in the absence of any other corrections, AIMD simulations will sample according to the microcanonical (NVE) ensemble. Most experiments are performed in a macroscopic setting where the samples are held at a constant temperature and a constant pressure or volume. Thermostats and barostats are used to regulate dynamics simulations to enable the sampling of an ensemble other than the microcanonical. The Nosé−Hoover thermostat,[16−19] a dynamical friction-based thermostat, and the stochastic thermostat of Andersen[20] have been used in the past to maintain a constant temperature. If the formulation of AIMD due to Car and Parrinello[3,7,21] is applied, as is the case here, then wave function kinetic energies may also be controlled by a Nosé-type thermostat or simply by imposing a constant friction force. A suitable thermostat in combination with a constant volume unit cell will give a simulation that samples the canonical (NVT) ensemble. Alternatively, the isothermal−isobaric (NPT) ensemble could be sampled under the control of a thermostat and a barostat. The systems of interest in the present study are all rather small making the application of a barostat difficult. We therefore limit ourselves to the canonical ensemble.

The technique of thermodynamic integration may be used to determine Helmholtz free energy differences from simulations that sample the canonical ensemble. If s is a running parameter for the progress along the reaction coordinate, then the free

* Author to whom correspondence should be addressed. E-mail: ziegler@ucalgary.ca.

10.1021/jp036007v CCC: $27.50
Published on Web 02/26/2004

energy change from one state, *a*, to a second state, *b*, is given by

$$\Delta_{a\rightarrow b}A = \int_a^b \left\langle \frac{\partial E(X,s)}{\partial s} \right\rangle_s \mathrm{d}s = -\int_a^b \langle F_s \rangle_s \, \mathrm{d}s \qquad (1)$$

where E represents the potential energy of the system as a function of the $3N$ spatial coordinates, X, with constraint s. F_s is the force acting on the chosen constraint. The brackets indicate an ensemble average of the system at the constraint value of the subscript s. The simple formula in eq 1 is correct for certain types of reaction coordinates including those used here. For a general reaction coordinate a more complicated formula is necessary.[14] The integral of eq 1 is typically evaluated through a finite difference numerical integration scheme.

Two possible methods to obtain the force data are the slow-growth (STI) and point-wise (PTI)[15] thermodynamic integration. In the slow-growth approach, the parameter s is changed by a very small amount every time step from state *a* to state *b*. The value of the ensemble average of the force at each value of s is then taken to be the value of the single force at that time step. The STI method is operated under the assumption that if the system is in equilibrium at the initial state *a*, then, if the change in s for each time step is small enough, the system will retain the equilibration. In the PTI method, a small number of points along the reaction coordinate are chosen and the system is allowed to dynamically evolve and sample phase-space at each point for a long time with no data collected between each point. The average force at each point is then used as the ensemble average of the force in eq 1. The PTI method ensures that equilibration of the system is kept throughout the reaction. A common problem with the STI method is that of free energy hysteresis[6,22] where the free energy profiles of the reaction simulated in both the forward and reverse directions differ by up to several kcal/mol. This hysteresis can only be eliminated by new and larger slow-growth simulations. On the other hand, for the PTI procedure one can simply add more discrete points until convergence of the integration is achieved or simulate longer at any given point to improve equilibration at that point. The two sampling methods discussed here should converge to the same answer in the limit where the number of times steps (for both methods) and points along the reaction coordinate (for the PTI method) approach infinity.

Methodology and Computational Details

In all cases, simple a priori reaction coordinates, namely atom−atom distances and center-of-mass distances were used in contrast to an a posteriori reaction path such as the IRC by Fukui.[23] This was deemed adequate because of the simplicity of the reactions studied.

The Car−Parrinello projector augmented-wave (CP−PAW)[24,25] program by Blöchl was used for all AIMD calculations. In addition to Car−Parrinello AIMD, Born−Oppenheimer dynamics[7] are often performed in combination with a quantum mechanical treatment of the electronic structure.[81−84] We think it is likely that the conclusions of the present work can equally be applied to BO−AIMD.

A typical simulation includes the following steps. The minimum in the potential energy hypersurface of the reactants or products and the corresponding wave function were obtained first. The reaction constraint is then introduced, and the system is thermally excited to a temperature of 300 K by exciting the normal modes of the system by a series of short orthogonal, sinusoidal energy pulses. The system is then equilibrated for at least 3 ps and often 5 ps or more depending on whether important properties, such as average temperature and average force on the constraint, were sufficiently stable.

Once equilibrium has been established, the reaction dynamics modeling is carried out. In the STI method, the system is moved a small amount along the reaction coordinate at every time step while the force along the constraint, F^j, is evaluated at each time step. The reaction is modeled in both the reverse and the forward directions. The reactions were remodeled with increasing numbers of time steps until the convergence of the forward and reverse reaction curves was acceptable and the free energy hysteresis was within desired error bounds.

The alternate to the STI sampling technique, the PTI method, also involves obtaining forces along the reaction constraint and numerically integrating to find the free energy change. Typically, data was accumulated at 15−35 points along the reaction coordinate for at least 30 000 time steps (3 ps) at each point to average the forces. To obtain the initial geometry, wave function, and velocities at each point along the reaction coordinate, a short slow-growth calculation was performed with input files saved at appropriate points. The first half of the time steps at each point were not included in the force average as they were considered performed only to allow the system to fully reequilibrate. Because a large number of points were available along the STI curve, it was integrated using the simple linear trapezium method, whereas the quadratic Simpson's method was used for the PTI integration where fewer points were available.

In the CP−PAW calculations, periodic boundary conditions were used in all examples with an orthorhombic unit cell described by the lattice vectors ([0, 14.74, 14.74], [14.74, 0, 14.74], [14.74, 14.74, 0]) (bohr, 7.8 Å) with the exception of the simulation of the dimerization of ketene which utilized a slightly larger ([0, 17.01, 17.01], [17.01, 0, 17.01], [17.01, 17.01, 0]) (bohr, 9.0 Å) cell. The energy cutoff used to define the basis set was 30 Ry (15 au) in all cases. Because the systems of interest are all isolated molecules, only the Γ-point in k-space was included and the interaction between images was removed by the method proposed by Blöchl.[25] The density-functional theory (DFT) functional used was that formed by the combination of the Perdew−Wang parametrization of the electron gas[26] in combination with the exchange gradient correction presented by Becke[27] and the correlation correction of Perdew.[28] The SHAKE algorithm[29] was used to impose constraints. The mass of hydrogen atoms was taken to be that of deuterium, and normal masses were taken for all other elements except where noted.

All CP−PAW calculations were performed at a target temperature of 300 K. All simulations controlled by a Nosé thermostat included a thermostat acting on the kinetic energy of the wave function. Unless otherwise noted, the characteristic frequency of the thermostat degree of freedom was 30.0 THz for the nuclear thermostat and 150.0 THz for the electronic thermostat.

The Andersen thermostat was applied to the nuclear motion by reassigning the velocity of N randomly chosen nuclei every n steps where N and n are chosen to maintain the desired temperature. In the case of the water−borane simulation this amounted to one velocity reassignment every 50 time steps. For the butadiene + ethene Diels−Alder reaction the reassignment was applied every 10 time steps. The 1,3-cyclopentadiene + ethene Diels−Alder reaction involved two reassignments every 10 time steps, the 5-amino-1,3-cyclopentadiene + ethene Diels−Alder reaction was carried out with two reassignments every 5 steps, the cyclopropanation used one reassignment every 20

steps, and the ketene dimerization required one reassignment every 30 time steps. Thermostat settings were monitored and adjusted as necessary during the equilibration stage, with the main criteria for adequate thermostating being the mean temperature lying within a range of 300 ± 10 K and a temperature drift lower than 1 K/ps. In combination with the Andersen thermostat, a constant friction was applied to the wave function with a value of 0.001 except in the case of the substituted Diels−Alder reaction where a value of 0.002 was used.

Although the Andersen thermostat is not commonly used in AIMD simulations, its application presents no particular practical challenges. Some care must be taken that the fictitious kinetic energy of the wave function does not become too large as, in our experience, the stochastic collisions cause it to increase somewhat. This increase was not too drastic for the systems studied here but may become a problem for larger molecules where a greater number of collisions would be necessary to maintain a desired temperature. It should be recalled that, owing to its stochastic nature, the Andersen thermostat should not be used when deterministic properties of trajectories in phase-space are of interest. This issue has no effect in the present study since deterministic trajectories are not required for the calculation of free energies, which are ensemble averages.

The water−borane complexation reaction was modeled with a time step of 7 au, the butadiene + ethene Diels−Alder reaction had a time step of 5 au, the other Diels−Alder reactions were studied with a time step of 7 au, the cyclopropanation reaction used a time step of 8 au, and the time step for the dimerization of ketene was 5 au (5 au ≈ 0.12 fs). The carbene reaction was performed with the carbene restricted to a singlet state. The internal energy curve of each reaction was obtained by a series of simulations where the nuclei and wave function were cooled to 0 K.

For the purposes of comparison, frequency analyses of the reactants, products, and (if possible) transition state geometries of each reaction were performed with the ADF program.[30−32] The functional used in the ADF calculations was very similar to that of the AIMD calculations. The gradient corrections were identical, but the parametrization of the homogeneous electron gas was that given by Vosko et al.[33] A TZ2P basis set was used in all static calculations. The integration accuracy was 10^{-6}, and geometry convergence criteria were 0.00002 au in the energy and 0.0003 au in the gradients. Atomic masses were identical to those used in the AIMD calculations.

Although the advantages of thermodynamic integration over a frequency analysis in the calculation of free energy differences have been noted, the reactions investigated here have been chosen such that the reactant and product molecules are for the most part relatively rigid. Frequency analyses should therefore provide excellent estimates of the free energies of these species and thereby good overall free energies of reaction with which comparisons can be made. Comparisons will also be made with free energies of activation derived from frequency analyses. The transition states are likely to be less rigid than the reactant or product molecules, and frequency analyses should provide less certain, though probably still reasonable, results for comparison.

Theoretical Details

The reactions discussed in this paper are modeled by starting with the reactants separated by a large distance (reaction coordinate value of 9.449 bohr (5 Å)) and then being brought together to form the product. When the reagents are separated by approximately 9.5 bohr, the intermolecular interaction is assumed to be negligible for the neutral reactants. This assumption was monitored by the criterion that the constraint force used was, on average, close to zero at the largest value of the reaction coordinate. Three constraints are applied to the system. First, the constraint corresponding to the reaction coordinate is included. Second, no translation of the center of mass of the whole system is allowed. Third, rotation of the total system about the center of mass is constrained. The entropic contributions to the reaction free energy need to be corrected for this finite separation and removal of translation/rotation in order to enable correct reaction free energies to be calculated.

The translational partition function is[34]

$$q_{\mathrm{T}} = \left(\frac{2\pi MkT}{h^2}\right)^{3/2} V \tag{2}$$

where M is the total mass of the system or reagent in question and V is the volume of the system. From eq 2, the translational entropy contribution is

$$S_{\mathrm{T}} = R\left(\ln(q_{\mathrm{T}}) + \frac{5}{2}\right) \tag{3}$$

The translational entropy at all stages of a simulation from reactants at a reaction coordinate of 9.449 bohr to the product is taken to be that corresponding to the total mass of the two reacting molecules at 300 K. The translational entropy of the reactants in a bimolecular addition reaction is usually taken to be the sum of the two reactant entropies.[34] The correction to the total entropy change due to translation is then found by subtracting the translational entropy of the reactants from the translational entropy of the products.

The rotational partition function of a system is given as[34]

$$q_{\mathrm{r}} = \frac{\pi^{1/2}}{\sigma_{\mathrm{r}}}\left(\frac{2kT}{\hbar^2}\right)^{3/2}(I_x I_y I_z)^{1/2} \tag{4}$$

where σ_{r} is the symmetry number representing the rotational degeneracy of the system and the terms I_α, for $\alpha = x, y$, and z, are the moments of inertia about the orthogonal axes x, y, and z. As in eq 3, the rotational entropy contribution is

$$S_{\mathrm{r}} = R\left(\ln(q_{\mathrm{r}}) + \frac{3}{2}\right) \tag{5}$$

Unlike the translational entropy, the rotational entropy is geometry dependent because the moments of inertia depend on the positions of the masses. Therefore, the amount of rotational entropy removed by the constraint that the total system cannot rotate varies as the reaction coordinate varies. Finally, as has already been noted, at the largest value of the reaction coordinate the reactant molecules are assumed to be noninteracting and to vibrate and rotate as though they were isolated molecules. The total entropy of internal motion of the system at this point on the reaction coordinate is therefore assumed to equal the sum of the vibrational and rotational entropies of the isolated molecules.

Thus, in a simulation of the reaction A + B → AB the overall entropy correction from isolated reactants to a reaction coordinate of s is

$$\Delta S^{\mathrm{AB}}_{\mathrm{PAWcorr}}(s) = S^{\mathrm{AB}}_{\mathrm{r}}(s) + S^{\mathrm{AB}}_{\mathrm{T}}(s) - S^{\mathrm{A}}_{\mathrm{T}}(\infty) - S^{\mathrm{B}}_{\mathrm{T}}(\infty) \tag{6}$$

It is clear that the free energy change $\Delta A^{\mathrm{AB}}_{\mathrm{PAW}}(s)$ obtained from a CP−PAW simulation with the constraints described above

must be corrected by $-T\Delta S_{\mathrm{PAW\ corr}}$ in order to obtain the total classical free energy change

$$\Delta A^{\mathrm{AB}}_{\mathrm{CM}}(s) = \Delta A^{\mathrm{AB}}_{\mathrm{PAW}}(s) - T\Delta S^{\mathrm{AB}}_{\mathrm{PAWcorr}}(s) \qquad (7)$$

where CM (classical mechanics) refers to the fact that the motion of the nuclei is described using classical mechanics in the calculations described here.

It should be noted that once a simulation has been performed the calculation of $\Delta S^{\mathrm{AB}}_{\mathrm{PAWcorr}}$ is very straightforward because the translational terms depend only on the nuclear masses and the temperature, and the rotational term depends only on the masses of the molecules, the temperature, and the geometry at the point of interest.

It might be thought that constraining the overall rotation and translation of a system may require further corrections to another part of the Helmholtz free energy of a reaction, ΔU_{T} (the contribution to the internal energy due to the heat capacities of translation, rotation, and vibration). However, in a classical description each degree of freedom will have an energy of $^1/_2RT$ irrespective of its type. In a reaction A + B → AB the number of degrees of freedom is equal to $3N$ on both sides of the equation where N is the number of atoms in molecule A plus the number of atoms in molecule B. Therefore, classically $\Delta U_{\mathrm{T}} = 0$. This is also the case in the simulations since the number of degrees of freedom is the same $(3N - 7)$ at all times. In a quantum mechanical description ΔU_{T} may not be zero since the energy of the vibrational modes is not likely to be $^1/_2RT$ at 300 K. We do not correct for this in the present work because calculating ΔU_{T} with standard formulas[34] requires recourse to the harmonic approximation, something that we would like to avoid.

Another contribution to ΔA that is not included in our simulations is the change in the zero-point energy (ZPE). There is no straightforward way for ΔA_{ZPE} to be added to the free energy curves derived from our simulations. If not for all points along the reaction coordinate, it can be added to the total reaction free energy change using the results of frequency analyses of the reactant and product molecules.

We thus will have several values for the change in free energy of a reaction: $\Delta A_{\mathrm{PAW}}(s)$, which comes directly from the thermodynamic integration, $\Delta A_{\mathrm{CM}}(s)$, which is $\Delta A_{\mathrm{PAW}}(s)$ corrected as in eq 7, ΔA_{QM}, which is derived directly from a frequency analysis, and finally $\Delta A_{\mathrm{QM}'}$, which is identical to ΔA_{QM} but with ZPE neglected and $\Delta U_{\mathrm{T}} = 0$. $\Delta A_{\mathrm{QM}'}$ should be directly comparable with ΔA_{CM}.

Results and Discussion

$BH_3 + H_2O \rightarrow H_2O{\cdot}BH_3$. The first reaction that we shall discuss is the formation of the Lewis acid−base complex of borane and water. This reaction is not of great interest experimentally since the H_2OBH_3 molecule is not found to be stable. It is a good subject for the present study, however, as it includes a very small number of atoms allowing a more extensive series of tests of the computational approaches under discussion. The reaction has not been studied exhaustively previously. The most important work for purposes of comparison with the calculations described here can be found in ref 35.

The reaction coordinate is chosen to be the oxygen−boron intermolecular distance. The reaction steps are shown graphically in Figure 1a. STI calculations requiring 50 000, 100 000, 200 000, 400 000, and 800 000 time steps were performed using both Nosé−Hoover and Andersen thermostats. PTI calculations were performed using only the Andersen thermostat. In this case 10 000 time steps is equivalent to about 1.7 ps.

The convergence of ΔA with respect to the number of steps in an STI calculation will be considered first. The free energy profiles of the 800 000 time step STI simulations are presented in Figure 1, parts b and c. Under Nosé thermostat control, the 50 000 time step STI hysteresis in ΔA between the forward and backward simulations was 3.2 kcal/mol with an average uncorrected value of ΔA_{PAW} of −8.6 kcal/mol. As the number of time steps increased, the hysteresis decreased to 2.5, 1.6, 0.8, and 0.3 kcal/mol for the 100 000, 200 000, 400 000, and 800 000 time step simulations, respectively. The corresponding results for the Andersen thermostat-controlled simulation were −0.4, 1.1, −0.6, −1.3, and −0.4 kcal/mol. The Nosé thermostat calculations appear to be fairly well converged by the 400 000 time step stage, whereas simulations run with the Andersen thermostat appear to do a little better and are fairly well converged by the 200 000 time step calculation.

We turn now to the convergence of the PTI calculations with respect to the length of the simulation at each value of the constraint. The Andersen PTI calculations were performed at 18 points in total for 50 000 times steps at each point. The equilibration was tested by comparing values of the force on the constraint averaged over the second half of a simulation starting with total run lengths of 10 000 time steps increased by 10 000 time steps (1.7 ps) each time. The uncorrected results of the 10 000, 20 000, 30 000, 40 000, and 50 000 time step PTI calculations are $\Delta A_{\mathrm{PAW}} = -9.7$, −10.2, −9.7, −9.5, and −9.9 kcal/mol, respectively. This suggests a reasonable convergence even after 10 000 time steps at each point along the reaction coordinate. The converged value is also in good agreement with the value of ΔA_{PAW} obtained from the STI calculations. The good agreement is further demonstrated in Figure 1d where the mean forces found at each increase in time step are shown in comparison with the force data from an 800 000 step Andersen-controlled STI simulation. The PTI points run through the middle of the oscillations in the force of the STI.

The electronic energy and free energy curves shown in Figure 1e offer qualitative insight into the reaction. On the electronic energy curve, the reaction has no barrier and has an early decrease in energy, starting at 8 bohr. This indicates a significant dipole−quadrupole interaction between the water and borane molecules. The minimum in the electronic energy curve corresponds to a binding energy of 14.2 kcal/mol. In contrast to the electronic energy, the free energy does not begin to decrease below the level of the reagents until the reaction coordinate reaches 6 bohr. The difference of approximately 3 kcal/mol between the two curves at 6 bohr indicates a significant entropic effect in the reaction. The free energy curve in fact has a maximum of about 1 kcal/mol at a value of the reaction coordinate of around 6 bohr, but given the accuracy of methods used here, it is not possible to be certain that a maximum should be present at all.

The conclusive ΔA_{PAW} value will be from the 50 000 time step PTI simulation. Once this is corrected to include entropic contributions according to eqs 6 and 7 we obtain $\Delta A_{\mathrm{CM}} = -6.5$ kcal/mol. Free energies of reaction can of course be calculated using the more conventional approach of frequency analysis.[34,36] This was done, and if, as described in the previous section, only the classical contributions to the nuclear energy are included, a free energy change $\Delta A_{\mathrm{QM}'} = -5.8$ kcal/mol is obtained in good agreement with ΔA_{CM}. The various changes in free energy (ΔA_{PAW}, $\Delta A_{\mathrm{PAW\ corr}}$, ΔA_{CM}, $\Delta A_{\mathrm{QM}'}$, and ΔA_{QM}) based on PTI are

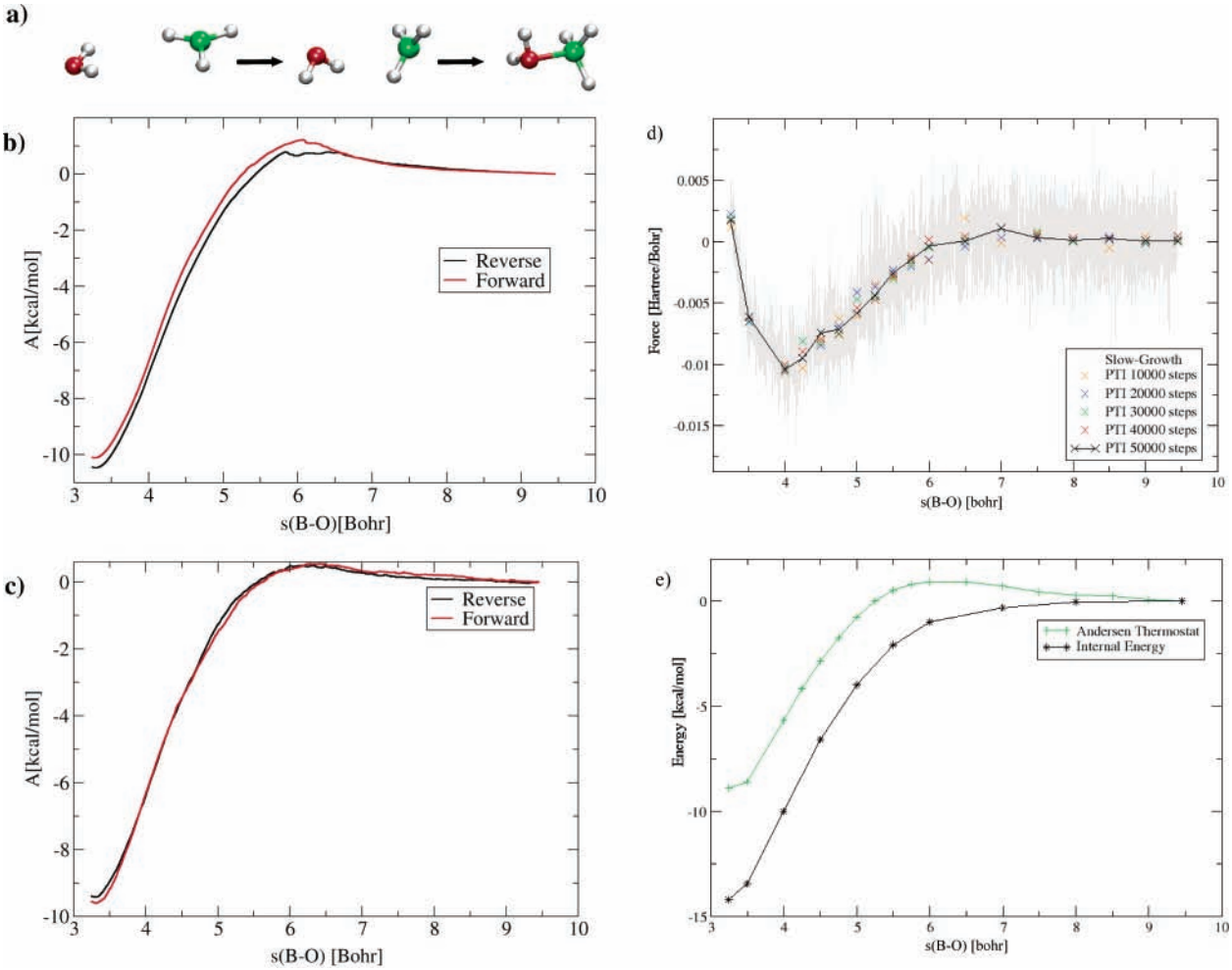

Figure 1. $BH_3 + H_2O$ complexation reaction. Part a shows the product complex, an intermediate separation (6.0 bohr, 3.2 Å), and full separation (9.4 bohr, 5 Å). Part b shows the 800 000 step STI Helmholtz free energy, *A*, profiles for the simulation with the Nosé thermostat. Part c shows the 800 000 step Andersen-STI. Part d shows the Andersen-PTI mean forces in comparison to the forces of the reverse Andersen-STI simulation. The STI forces are given as a running average of window width of 250 time steps or approximately every 0.001 Å change of the B−O distance, and the 50 000 time step PTI points are represented by the gray line. Part e shows the PTI free energy curve and the 0 K internal energy curve, both adjusted to have a value of zero at a separation of 9.4 bohr (5 Å).

TABLE 1: Free Energy Changes for the Reaction A + B→ AB Found from PAW from Simulation with the PTI Method, Correction Terms, and Comparison Static (ADF) Calculations

reaction	thermostat	ΔA_{PAW}	$\Delta A_{corr}{}^{a,e}$	$\Delta A_{CM}{}^{b,e}$	$\Delta A_{QM'}{}^{c,e}$	$\Delta A_{QM}{}^{d,e}$
$BH_3 + H_2O \rightarrow H_2O{\cdot}BH_3$	Andersen	−9.9	3.4	−6.5	−5.8	−2.9
Diels−Alder (butadiene)	Nosé	−32.0		−29.6		
	Andersen	−28.8	2.4	−26.4	−26.3	−22.6
Diels−Alder (cyclopentadiene)	Nosé	−17.4		−15.0		
	Andersen	−8.6	2.4	−6.2	−6.0	−2.6
Diels−Alder (anti addition)	Nosé	−19.1		−16.9		
	Andersen	−11.5	2.2	−9.3	−9.2	−5.9
Diels−Alder (syn addition)	Nosé	−21.8		−19.6		
	Andersen	−13.1	2.2	−10.9	−9.9	−6.7
cyclopropanation	Nosé	−56.9		−54.5		
	Andersen	−48.2	2.4	−45.8	−48.3	−44.9
2ketene → diketene	Andersen	−8.2	2.7	−5.5	−5.9	−2.3
2ketene → cyclobutadione	Andersen	−7.2	2.7	−4.5	−3.0	−0.2

[a] Correction from eq 9. [b] ΔA_{PAW} corrected as in eq 9. [c] From frequency analysis without ZPE and the QM part of the vibrational internal energy contributions. [d] From frequency analysis including all contributions. [e] Energies are reported in kcal/mol.

given in Table 1 for the $BH_3 + H_2O$ reaction (as well as the other reactions discussed here). The corresponding internal energy changes of all reactions are given in Table 2.

In the previous study of this reaction[35] the complexation energy of BH_3 and H_2O was calculated at the G2 level and found to be 10.3 kcal/mol. This result includes ZPE and is, therefore, with the ΔU_{QM} value of 11.9 kcal/mol from Table 2.

Diels−Alder Cyclizations. The Diels−Alder reaction is perhaps the prototypical example of a cycloaddition reaction between two nonpolar molecules. It has been studied extensively

TABLE 2: Internal Energy Changes for the Reaction A + B→ AB in kcal/mol

reaction	ΔU_{PAW}	ΔU_{QM}, [a]	ΔU_{QM} [b]
$BH_3 + H_2O \rightarrow H_2O{\cdot}BH_3$	−14.2	−14.8	−11.9
Diels−Alder (butadiene)	−41.0	−41.5	−37.8
Diels−Alder (cyclopentadiene)	−20.0	−20.0	−16.6
Diels−Alder (anti addition)	−24.5	−24.3	−21.0
Diels−Alder (syn addition)	−24.6	−24.9	−21.7
cyclopropanation	−61.0	−61.6	−58.2
2ketene → diketene	−20.7	−19.9	−16.3
2ketene → cyclobutadione	−17.3	−16.2	−13.4

[a] From frequency analysis without ZPE and the QM part of the vibrational internal energy contributions. [b] From frequency analysis including all contributions.

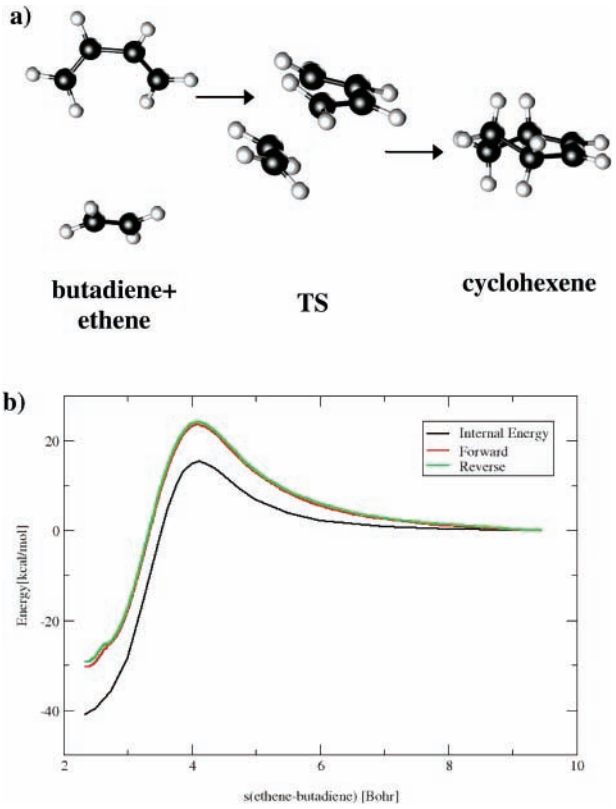

Figure 2. Diels−Alder reaction of butadiene and ethene. Part a shows the reagents, the transition state (TS), and the product. Part b shows the internal energy curve and the STI free energy curves from the forward and reverse 800 000 time step simulations.

by theoreticians with the major points of interest being the structure of the transition state and the question of whether it follows a concerted or stepwise mechanism (see refs 37−44 and references therein). In the present study, the Diels−Alder reaction is a logical second step. Like the $H_2O + BH_3$ reaction, it is relatively simple and involves a small number of atoms. In contrast to $H_2O + BH_3$, however, the Diels−Alder cyclization has a significant enthalpic barrier making it a somewhat different problem from the point of view of dynamics simulations. Four Diels−Alder reactions were studied: butadiene and ethene (Figure 2), cyclopentadiene and ethene where the diene is constrained to be in the cis conformer (Figure 3), and the syn and anti reactions between ethene and 5-amino-1,3-cyclopentadiene (Figure 4). These last two reactions were chosen in order to see what dynamics calculations can tell us about the stereoselectivity of the Diels−Alder reaction.

The reaction coordinate chosen in all cases was the distance between the center of the C−C double bond in ethene and the

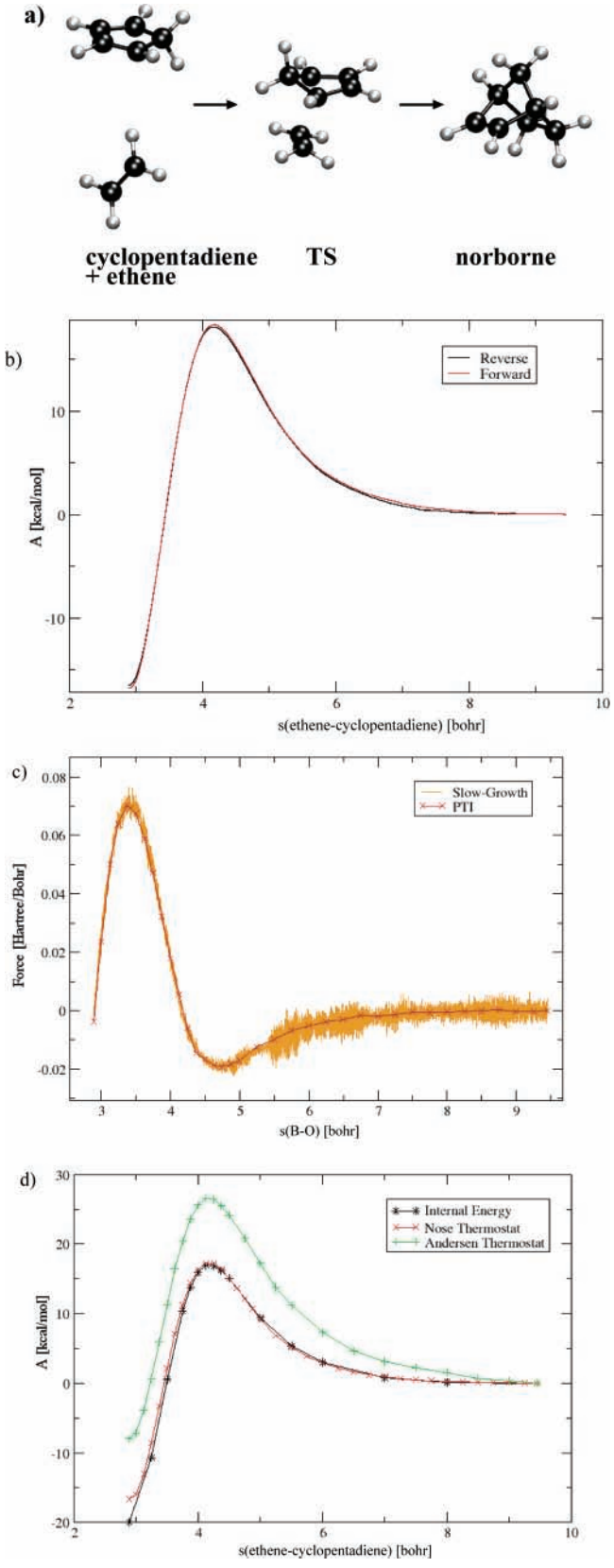

Figure 3. Diels−Alder cycloaddition of cyclopentadiene and ethene. Part a shows the reagents, the transition state (TS), and the product. Part b gives the 400 000 time step STI free energy curves for the Nosé thermostat-controlled reaction. Part c gives a comparison of the forces obtained in the 400 000 time step Nosé-TI calculation, presented as a running average with a window of 250 time steps and the mean forces for the PTI calculation. Part d gives the free energy profiles calculated by the PTI method and the internal energy profile, where both curves are set to zero as a reference at a separation of 9.4 bohr (5 Å).

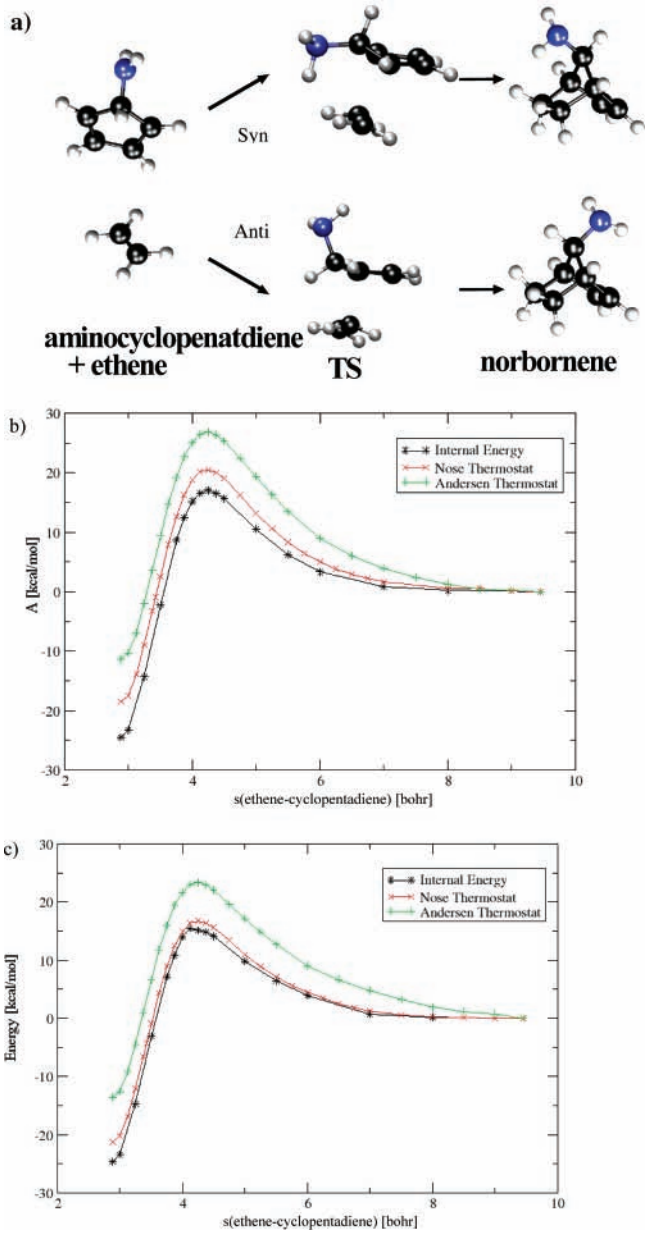

Figure 4. Stereoselective Diels−Alder cycloadditions of aminocyclopentadiene and ethene. Part a shows the syn addition (top) and the anti addition (bottom). Part b shows the PTI free energy profiles for the anti addition for both Nosé and Andersen thermostats as compared to the internal energy curve. Part c shows the Nosé thermostat PTI free energy curve and internal energy curve for the syn addition. Energy curves are set to zero at 9.4 bohr (5 Å).

midway point between the two carbons of the diene which will form new σ bonds.

The convergence of the slow-growth procedure was tested for the Diels−Alder reactions of ethene with butadiene and cyclopentadiene. Simulations controlled by both thermostats were performed in both forward and reverse directions with 50 000, 100 000, 200 000, and 400 000 time steps. The results of these calculations are presented in Table 3.

Two striking results are apparent from the data in Table 3. First, the hysteresis in the calculations of the butadiene + ethene reaction is much greater than that of the cyclopentadiene + ethene reaction. The cyclopentadiene + ethene results are similar to those of the $BH_3 + H_2O$ reaction where the hysteresis is never greater than 4 kcal/mol and suitable convergence is reached by the 200 000 or 400 000 time step calculations. The calculation using the Nosé thermostat in fact appears to be converged already with the 50 000 time step calculation. In contrast, the hysteresis in both of the 50 000 time step calculations of the butadiene + ethene reaction is as large as 19 kcal/mol. With the Nosé thermostat, the forward and reverse simulations agree well with each other once 400 000 time steps are included. The hysteresis in the Andersen calculation is a still unsatisfactory 3 kcal/mol in the 400 000 time step calculation. To try to improve on this result, a computationally demanding 800 000 time step (96 ps) simulation was run with just the Andersen thermostat. The hysteresis in this calculation is a more acceptable 1.0 kcal/mol. The free energy curves from the 800 000 time step STI calculations along with the internal energy curve are presented in Figure 2b.

To understand why the STI method performs so poorly for the butadiene + ethene Diels−Alder reaction in comparison with the cyclopentadiene + ethene or $BH_3 + H_2O$ reactions, one must consider the mechanism of the reactions in question. The transition state of a Diels−Alder reaction has the atoms that are forming a six-membered ring in a C_s-symmetric arrangement where the dieneophile approaches the diene from one side (Figure 2a). To proceed from the transition state to products in the case of the butadiene + ethene reaction, the two former ethene carbons must twist in such a manner as to give the final C_2 symmetry of cyclohexene. This twisting motion involves very little change of our chosen reaction coordinate, which is the distance between the midpoint of the ethene C−C bond and the halfway point between the two terminal carbons of the butadiene molecule. This reaction coordinate is therefore quite a poor choice for this part of the reaction and, as we have seen from the results in Table 3, requires a lot more effort to produce correct results. The transition from the C_s-type structures to the C_2-type structures shows up as a small shoulder on the free energy curves in Figure 2b. Norbornene has C_s symmetry like the transition state for its formation and the B−O distance is obviously a good choice of reaction coordinate for the $BH_3 + H_2O$ reaction, so similar problems do not arise for these two reactions. The butadiene + ethene example is demonstration of the need to choose a good reaction coordinate when calculating reaction free energies using thermodynamic integration. For systems more complicated than those studied here it often may become mandatory to use a more versatile reaction coordinate such as an intrinsic reaction coordinate (IRC).[23,45]

The second interesting result from the data in Table 3 is the fact that the simulations controlled by the Nosé thermostat do not give the same value for ΔA_{PAW} of the ethene + cyclopentadiene reaction as the simulations controlled by the Andersen thermostat even when very large numbers of time steps are used. The obvious first question is which, if any, of the calculations is correct. From the static frequency calculations code $\Delta A_{QM'}$ is determined to be −6.0 kcal/mol. ΔA_{PAW} (Nosé) is taken as the average of the forward and reverse 400 000 time step STI simulations giving −16.7 kcal/mol. In a similar fashion ΔA_{PAW} (Andersen) are found to be −8.6 kcal/mol. Using eq 7 to convert the ΔA_{PAW} into ΔA_{CM}, we obtain ΔA_{CM}(Nosé) = −14.3 kcal/mol and ΔA_{CM} (Andersen) = −6.2 kcal/mol. The corrected Andersen results agree well with the value from the frequency analysis. The explanation as to why the Nosé thermostat performs to poorly will be deferred for a moment, as the PTI calculations provide clearer evidence for the discussion and therefore will be described first.

PTI calculations of both reactions using either of the thermostats were performed. The results of these calculations are summarized in Table 1.

TABLE 3: ΔA_{PAW} in kcal/mol of Diels−Alder Reactions Calculated by the STI Method

number of time steps	butadiene + ethene				cyclopentadiene + ethene			
	Nosé		Andersen		Nosé		Andersen	
	forward	reverse	forward	reverse	foreword	reverse	forward	reverse
50 000	−23.4	−34.9	−19.1	−38.3	−16.9	−17.4	−8.0	−5.4
100 000	−26.1	−37.9	−26.8	−36.2	−16.0	−16.3	−12.3	−9.8
200 000	−29.8	−33.5	−25.6	−29.1	−16.0	−16.9	−7.3	−8.7
400 000	−33.0	−33.9	−25.1	−28.1	−16.8	−16.5	−9.0	−8.3
800 000	*a*	*a*	−30.3	−29.3	*a*	*a*	*a*	*a*

[a] Calculation not performed.

To complete the outline of why the thermostats give differing results for the cyclopentadiene + ethene reaction, the PTI results for this system will be discussed first. The PTI values of ΔA_{PAW} for this reaction are −17.4 kcal/mol (Nosé) and −8.6 kcal/mol (Andersen) in disagreement with each other but in agreement with the equivalent STI result. The free energy profiles for the Diels−Alder reaction of cyclopentadiene with ethene based on PTI calculations with both the Nosé and Andersen thermostats and the 0 K internal energy curve are presented in Figure 3d. It is obvious that the free energy curve with the Nosé thermostat does not deviate from the internal energy curve with any real significance. All of the reactions discussed in this paper are addition reactions with large negative values of ΔS, and the internal energy and free energy curves should not coincide. The PTI and STI methods therefore give the same incorrect results, and the error cannot be attributed to the method of obtaining averaged forces.

Visual inspection of the Nosé-PTI calculation molecular trajectories showed that, at long separations, the individual molecules do not rotate in any appreciable manner. Thus, it appears that the rotational modes are not sufficiently excited by the Nosé thermostat in this case. This hypothesis was confirmed by a more quantitative analysis. Taking the point from each of the PTI calculations corresponding to the greatest separation of 9.449 bohr (5 Å), the motion of the ethene molecule was separated out. By use of standard formulas of classical mechanics,[46] the rotational motion of the ethene molecule was further separated and the kinetic energy about the principal axes determined. The nuclei in these simulations should be equilibrated at 300 K, and therefore, each rotational direction should have $^1/_2RT$ or 0.3 kcal/mol of energy. In the simulation controlled by the Nosé thermostat, the average energies in the rotational modes were 0.005, 0.005, and 0.006 kcal/mol. Furthermore, a line fitted through the total rotational energy as a function of time had a gradient of −0.01 kcal/mol ps, suggesting that the thermostat was not able to push the rotational modes toward equilibration. In contrast, the Andersen simulation produced trajectories that have the reactant molecules apparently rotating freely and gave more reasonable average rotational energies of ethene about its principal axes of 0.2, 0.3, and 0.2 kcal/mol.

The Nosé thermostat uses an extra degree of freedom that acts as a heat bath for the system of interest.[16] This extra degree of freedom has a chosen mass with a corresponding frequency for coupling with the other degrees of freedom. The thermostat currently implemented in the PAW program is an improvement on the original Nosé thermostat,[19] but it appears that it is unable to provide a wide enough frequency spectrum to equilibrate the cyclopentadiene + ethene system. It is certainly an improvement over the standard Nosé thermostat, which was implemented in older versions of PAW. Test calculations with this thermostat found it to be very poor for both butadiene + ethene and cyclopentadiene + ethene systems and a number of others systems to which it was applied. Possible modifications to the present Nosé thermostat which may improve its behavior include applying a thermostat to each particle[47] or using a chain of Nosé thermostats.[48−51] The Andersen thermostat of course does not suffer from a similar problem as an even distribution of energy among all degrees of freedom is implicit in its definition.[20]

Other possible causes for the poor performance of the Nosé thermostat may be the removal of the rotational motion of the overall system and a poor choice of the coupling frequency of the thermostat. The first possibility was tested by rerunning a simulation at a large value of the constraint of the amino-cyclopentadiene + ethene system with the overall rotation constraint removed. This led to nearly no change in the rotational kinetic energy of the individual molecules. To test the second possibility, a series of calculations of the same system were run with a range of characteristic frequencies of the nuclear thermostat from 1.0 to 200.0 THz. The rotational kinetic energy of the individual molecules did change somewhat as a function of the frequency but never approached the required value.

The lack of energy in the rotational modes of the reactants in the cyclopentadiene + ethene Diels−Alder reaction is responsible for the poor results obtained when it is simulated using the Nosé thermostat. As detailed in the previous section, the translational entropy of the isolated molecules is not included in the simulations but rotational entropy is. In the course of a simulation, this rotational entropy is lost leading to the majority of difference between the calculated internal and free energy curves ΔA_{PAW}. If the rotation of the reactants is not treated correctly, then the simulation cannot hope to give a reasonable free energy curve. Because the free energy curve from the Nosé-controlled simulation almost coincides with the internal energy curve, it is likely that the vibrational modes are also poorly equilibrated.

When the PTI results in Table 1 are compared with the STI reaction energies from Table 3, it is clear that both methods give very similar results (erroneous or not) for these two reactions. Although the simulation at each point of the PTI calculation lasted 30 000 time steps, all were mostly converged after only 10 000 time steps. The cyclopentadiene + ethene reaction again converged more rapidly, but the butadiene + ethene free energies of reaction were only in error by 1 kcal/mol when comparing the 10 000 time step per point with the 30 000 time step per point PTI calculations.

It has already been noted that the Andersen-controlled STI calculation of the cyclopentadiene + ethene reaction gives a free energy of reaction in good agreement with the energy obtained from static frequency calculations. It follows from Table 1 that an equally good agreement is obtained with the PTI scheme. What about the butadiene + ethene reaction? The best calculations, either PTI or STI give ΔA_{PAW} of about −29 kcal/mol (Andersen) and about −33 kcal/mol (Nosé). Again using eq 7 to convert ΔA_{PAW} into ΔA_{CM}, we obtain values near −26.5 kcal/mol (Andersen) and −30.5 kcal/mol (Nosé) which

may be compared with −26.3 kcal/mol from static calculations. Thus, it appears that the simulation of the ethene + butadiene Diels−Alder reaction with the Nosé thermostat may also underestimate the magnitude of ΔS.

It was noted at the beginning of this section that an important difference between the Diels−Alder reaction and the addition reaction between H_2O and BH_3 is the presence of an internal energy barrier. Although no special effort was made to find the location of the transition states on the internal energy curve, from interpolation of the available data points they are expected to be found at values of 4.10 au and 4.18 au of the reaction coordinate for the butadiene + ethene and cyclopentadiene + ethene reactions, respectively. The heights of the two barriers, $\Delta U^{\ddagger}$, are 15.3 and 16.9 kcal/mol above the reactants. In a manner similar to that used for the internal energy transition states, the free energy transition states were found by interpolation among the Andersen-controlled PTI points. The transition states are located at separations of approximately 4.08 and 4.19 bohr with values of $\Delta A^{\ddagger}_{PAW}$ of 24.9 and 26.0 kcal/mol, respectively, for the butadiene + ethene and cyclopentadiene + ethene reactions. Although the STI simulations could be used to locate the transition states without needing to resort to interpolation, the PTI results were taken here to be consistent with the rest of the reactions. Again using eq 7, the $\Delta A^{\ddagger}_{PAW}$ can be converted into $\Delta A^{\ddagger}_{CM}$ giving values of 28.2 and 29.2 kcal/mol. The entropic contributions to the free energy barriers are approximately 13 and 11 kcal/mol, respectively. The majority, but not all, of the entropy is thus lost at the transition state. The transition state occurs at the same value of the reaction coordinate on the internal energy scale as on the free energy scale.

Just as the free energy changes of reaction calculated from thermodynamic integration can be compared with equivalent values derived from frequency analyses, free energies of activation can be compared with results obtained from this source. Transition states of the two reactions in question were found using the ADF program and identical reaction coordinates to those taken for the dynamics calculations. The locations of these transition states were 4.08 and 4.17 bohr for the butadiene + ethene and cyclopentadiene + ethene reactions, respectively. Frequency analyses at these geometries confirm that they are indeed transition states. Each analysis gives real vibrational frequencies with the exception of one of about $400i$ cm^{-1}. $\Delta A^{\ddagger}_{QM'}$ calculated from the results of the frequency analyses are 28.7 and 29.9 kcal/mol in very good agreement with the values for $\Delta A^{\ddagger}_{CM}$ from the dynamics calculations.

Li and Houk have studied the barriers of the Diels−Alder reaction between ethene and butadiene in some detail.[40] From RQCISD(T)/6-31G* and UQCISD(T)/6-31G* calculations they obtain somewhat larger values of $\Delta U^{\ddagger}$ of 25.5 and 29.4 kcal/mol, respectively. In contrast, the entropic contribution to $\Delta A^{\ddagger}$ is found by these workers to be 12.8 kcal/mol in good agreement with the results given here.

The cycloreversion of norbornene to form ethene and cyclopentadiene was studied recently at the CASSCF/6-31G* and B3-LYP/6-31G* levels.[74] ZPE was included in these calculations, but entropy effects were not. The B3-LYP reaction energy and activation barrier from ref 74 (−18.4 and 22.4 kcal/mol) agree quite well with the present results. The agreement is poorer with the CASSCF results (−12.9 and 38.4 kcal/mol).

The other Diels−Alder cyclization reaction considered is ethene + 5-amino-1,3-cyclopentadiene → amino-norbornene which has recently been examined both experimentally[52] and theoretically.[44,53] This reaction is depicted in Figure 4a. Having established in the previous examples that the PTI method is comparable to the slow-growth scheme, the ease of implementing the PTI method drove us to restrict ourselves to the PTI method for the remaining systems. Simulations were run with both available thermostats; 28 points along the reaction curve were used for both syn and anti addition pathways with simulations totaling 30 000 time steps (5.1 ps) at each point. The free energy profiles of the simulations controlled by the Nosé thermostat are plotted along with the 0 K internal energy curves in Figure 4, parts b and c. The free energy profile of the syn addition pathway under Nosé thermostating clearly suffers from the same flaw as that shown by the cyclopentadiene + ethene calculation controlled by the same thermostat. Only minor entropic effects are found. Visual inspection of trajectories at longer separations confirmed that again no rotational motion was present. The Nosé-controlled anti addition pathway free energy profile does not suffer from this problem, or at least not in the same blatant fashion as the previous cases, as the final entropic contribution to ΔA_{PAW} is $\Delta(-TS) = 5.4$ kcal/mol. This entropic effect is somewhat smaller than might be expected, however. Visual examination of trajectories found that some rotational motion was present in this simulation for large values of the reaction coordinate.

The free energy curves derived from PTI calculations using the Andersen thermostat are also plotted in Figure 4, parts b and c. Both of the Andersen curves in parts b and c of Figure 4 lie well above the curves from the Nosé thermostat calculation implying that the Nosé thermostat does not perform well in this case either. Under Nosé thermostat control, the corrected PTI results are for the anti addition $\Delta A_{CM} = -15.0$ kcal/mol and for syn addition $\Delta A_{CM} = -16.9$ kcal/mol. The static result was $\Delta A_{QM'} = -9.2$ kcal/mol for the anti addition and $\Delta A_{QM'} = -9.9$ kcal/mol for the syn addition. Both Nosé-PTI results are too low, owing to the lack of rotational contribution to the entropic change in the reactions. The Andersen-controlled simulations give good agreement with the static calculated values with a corrected value of $\Delta A_{CM} = -9.3$ kcal/mol and $\Delta A_{CM} = -10.9$ kcal/mol for the anti and syn additions, respectively.

One of the major point of interest in the Diels−Alder reaction of ethene with 5-amino-1,3-cyclopentadiene is the possibility for π-facial selectivity. It has been found that the major product of the reaction of a dieneophile with 5-amino-1,3-cyclopentadiene corresponds to preferential approach to the syn face the diene.[52] The product distribution of these types of reactions is generally believed to be under kinetic control. Some rationalizations of the observed behavior focus on the properties of the reactants, whereas others deal with the properties of the transition states (see refs 44, 52, 54−58, and references therein). Ultimately, kinetic control implies that two competing processes have different free energies of activation, a quantity that can be obtained from the present calculations.

The transition state for the syn reaction was found to be at a value of 4.25 bohr of the reaction coordinate, whereas for the anti addition it was only negligibly different at 4.26 bohr. The corrected values of $\Delta A^{\ddagger}_{CM}$ are 28.9 and 25.9 kcal/mol for the anti and syn reaction, respectively. These results suggest that the syn addition will be favored over the anti reaction in agreement with experimental results. For the sake of comparison, the $\Delta U^{\ddagger}$ values obtained from these calculations are 17.0 and 15.1 kcal/mol with the transition state being at 4.25 bohr in both cases. Thus, entropy effects may increase the preference of syn addition over anti, but the change of 1 kcal/mol in the difference between the syn and anti reaction barriers is probably within the error bars of the present method and should not be given too much weight.

The entropic contributions to $\Delta A^{\ddagger}_{CM}$ are 12 and 11 kcal/mol for the anti and syn reactions, respectively. This constitutes 75−80% of the entropic change to the free energy changes of reaction implying that again most, but not all, of the entropy that is to be lost is gone by the time the reaction reaches the transition state. Static calculations were performed to provide comparisons with the calculated values of $\Delta A^{\ddagger}_{CM}$. The transition states located in this case are at 4.22 and 4.23 bohr and with energies of $\Delta A^{\ddagger}_{QM'} = 30.4$ and 28.3 kcal/mol, respectively, for the anti and syn reactions. The free energy barriers from frequency analyses are a little higher than those derived from dynamics calculations. It is not clear from where the discrepancy arises, since the free energy and internal energy transition states are predicted to be at almost identical values of the reaction coordinate and the frequency analyses include no frequencies below 100 cm^{-1}.

The activation energies of the syn and anti Diels−Alder reactions of aminocyclopentadiene and ethene were studied previously by Xidos and co-workers[44] at the HF/6-31G* level. Only the relative values of the activation energies were quoted in this work. The barrier leading to syn addition was found to be 1.7 kcal/mol lower in energy than that leading to anti addition in good agreement with the present results.

Cyclopropanation. The addition of a carbene to an alkene is an important reaction of divalent carbon and a useful route to cyclopropane ring structures. The reaction of a singlet carbene is believed to proceed in two phases starting with an electrophilic approach to the double bond followed by nucleophilic attack at one of the two alkene carbon atoms.[59] The reaction of dichlorocarbene with ethene has been found to proceed with a zero or even negative ethalpic barrier[60−62] with a free energy barrier that is believed to be largely entropic in origin. Theoretical studies have largely focused on whether a minimum corresponding to a weakly bound π-complex is present in the enthalpic reaction curve.[59,63−65] If such a minimum does exist then a transition state on the enthalpy curve can be present. The most accurate calculations available at this time suggest that no minimum corresponding to a π-complex exists, at least for the dichlorocarbene−ethene reaction.[65] It is well-known that DFT methods are not the best choice for describing weak long-range interactions and therefore, calculations of the type described in this paper cannot provide further insight into the question of the existence of a π-complex in the enthalpic reaction curves. However, the calculation of free energy curves is under discussion here, and a reaction such as that between CCl_2 and ethene where most, or even all, of the free energy barrier is due to entropic effects was chosen as another useful test case.

The reaction of dichlorocarbene + ethene → 1,1-dichlorocarbene was studied exclusively with the PTI method, using both Nosé and Andersen thermostats. The total electron spin of the system was constrained to be 0, corresponding to a singlet carbene. The singlet state is expected to be more stable[66] than the triplet state in this case of a dihalide carbene. The reaction coordinate chosen was the interatomic distance between the carbene carbon and the center of mass of the two ethene carbons. For the Nosé thermostat, a total of 22 points along the reaction curve was used. At each point a simulation 30 000 time steps (5.7 ps) in duration was performed. The corrected free energy change was found to be $\Delta A_{CM} = -56.3$ kcal/mol, and as is visible from the energy profiles shown in Figure 4b, the free energy curve did not deviate in any significant fashion from the 0 K internal energy curve. Upon visual inspection of the nuclear trajectories at the longer reagent separations, it was apparent that neither of the molecules was rotating about their respective centers of mass. This is again attributed to the Nosé thermostat unsuccessfully sustaining the energy of the rotational normal modes.

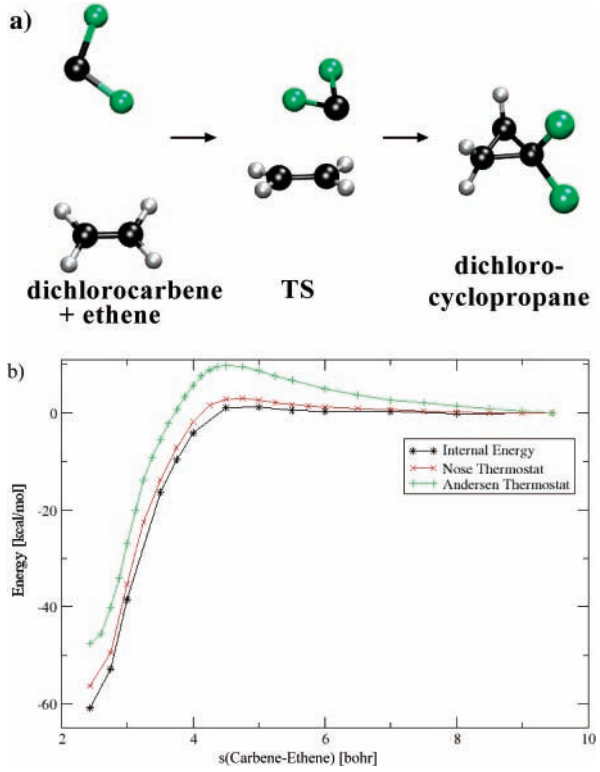

Figure 5. Cyclopropanation of ethene with dichlorocarbene. Part a shows the reagents, the transition state (TS), and product. Part b gives the free energy profiles calculated by the PTI method and the internal energy profile.

A total of 29 points along the reaction curve were used for the Andersen thermostat. While the PTI calculations of the previous reactions (with the exception of the butadiene + ethene Diels−Alder reactions) were close to converged after only 10 000 time steps and certainly converged by 30 000, the convergence of the PTI with the Andersen thermostat was somewhat slower. Starting at 10 000 times steps for each point, convergence of the free energy change was assessed at increments of 10 000 time steps until 60 000 time steps (11.4 ps) was reached. The ΔA_{PAW} results for the increasing number of times steps are, with the 9.449 bohr (5 Å) separation defined to be zero as a reference, $\Delta A_{PAW} = -47.0, -45.7, -46.8, -48.3, -47.6$, and -47.6 from least to greatest number of steps. Thus, convergence within ±1 kcal/mol by the 40 000 time step mark is suggested. The reason for the poorer convergence is the same as was the case for the butadiene + ethene reaction. The reaction proceeds with the carbene first approaching the two carbons equidistantly but soon veering nearer to one. The chosen reaction coordinate is a reasonable choice for this process. The two C−C bonds are formed stepwise. It is the formation of the second bond that is less well described by the reaction coordinate as it involves the three carbons going from a rough L-shape to the cyclopropane structure, a transformation that involves only a relatively small change in reaction coordinate.

From Figure 5b, it is clear that the free energy curve derived from the calculations controlled by the Andersen thermostat does deviate from the 0 K internal energy curve. Similar visual inspection of the nuclear trajectories revealed that the Andersen thermostat did successfully excite the rotational normal modes of the system.

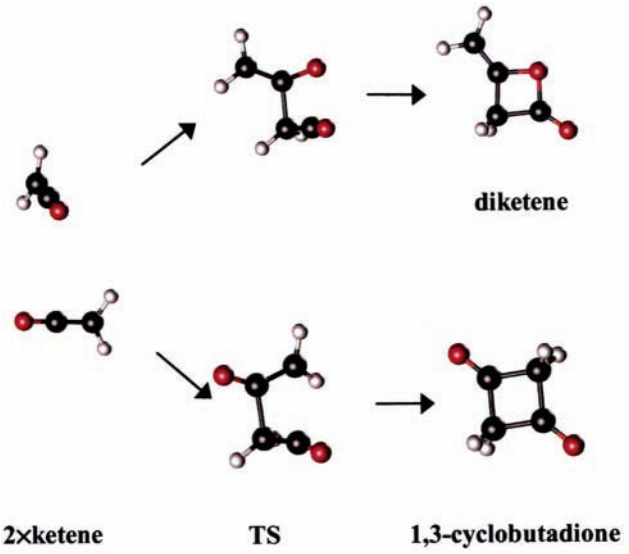

Figure 6. Dimerization of ketene.

Considering the 60 000 time step Andersen-PTI result as most accurate, the final, corrected answer is $\Delta A_{CM} = -45.8$ kcal/mol. The corresponding frequency analysis result is $\Delta A_{QM'} = -48.3$ kcal/mol, without ZPE correction, which indicates a small overestimation of the free energy change by the Andersen-PTI method. As is visible in Table 2, the internal energy differences found in both PAW and ADF are within ±1 kcal/mol; thus, this overestimation is due to the entropy change, ΔS, being overly negative in the PAW simulation.

The internal energy curve of Figure 5b does have a maximum at about 4.5 bohr, but as was noted earlier, the present method is not accurate enough to successfully describe such a small barrier. The free energy curve has a maximum at the same distance. Near the free energy transition state the calculated trajectories place the carbene nearer to one of the ethene carbons, in accordance with molecular orbital symmetry considerations[67] that would predict a very high barrier for a transition state with C_{2v} symmetry. The corrected free energy barrier $\Delta A^{\ddagger}_{CM}$ is 11.7 kcal/mol. The PTI method thus predicts a large entropic barrier for the reaction of dichlorocarbene with ethene in agreement with experimental results. This result is also in agreement with earlier frequency analysis calculations of the free energy barrier height[63,64] but disagrees somewhat as to the location of the transition states with the previous calculations giving values of 3.8 bohr[63] and less than 4.25 bohr.[64]

Dimerization of Ketene. The final reaction that will be discussed is the 2 + 2 cycloaddition of two ketene molecules. The ketene functional group is highly reactive and is used to form cyclobutane rings through 2 + 2 cycloaddition reactions with alkenes. It is so reactive that it often reacts with itself in a 2 + 2 fashion to form a 1,3-cyclobutadione. The simplest possible ketene, commonly called ketene, is somewhat exceptional in that even in the absence of a catalyst it mainly (95%) dimerizes to form methylene-β-propiolactone (diketene),[68] Figure 6a, with only a small amount (4−5%) of the dione formed.[69] A few computational studies of the dimerization of ketene have been published, mainly looking at the structure of the transition state and why the lactone is the major product rather than 1,3-cyclobutanedione.[70−72]

It may seem initially that dimerization of ketene does not offer anything new as a test case when compared with the other reactions discussed here. However, it turns out that studying this reaction using thermodynamic integration does create some new difficulties due to the possibility of a bifurcation in the reaction path.

The PTI method in combination with the Andersen thermostat is now well established as our method of choice for calculating free energies curves. It was applied to the formation of diketene with the chosen reaction coordinate being the distance between the midpoint of the C−C double bond of one ketene molecule to the midpoint of the C−O double bond of the other ketene molecule. Unfortunately, at present the PAW program does not offer the option to constrain distances with respect to the midpoint between atoms but rather allows the distance between the centers of mass of two groups of atoms to be constrained. In all previous examples, the midpoints between atoms that formed part of the constraints were the midpoint between two atoms of the same element. In this case, the center of mass of these two atoms is the midpoint between them allowing the calculation to proceed with no difficulties. For the diketene reaction, one of the midpoints is halfway between an oxygen atom and a carbon atom. To get around this problem the masses of the carbon and oxygen atoms in this simulation were artificially chosen to be equal to each other at 12.0 amu. The use of incorrect masses for the oxygen atoms should not introduce any significant errors since it has been shown that configurational averages derived from dynamics calculations are independent of the masses chosen for the atoms.[73]

The reaction of two diketene molecules to form the 1,3-cyclobutanedione was also studied with the PTI procedure. In this case, the reaction coordinate was chosen to be the distance between the midpoint of the C−C double bond of each monomer molecule. Obviously, it was not necessary to assign an unusual mass to the oxygen atom in this case.

Simulations of 30 000 (3.6 ps) time steps in duration were performed at each point of the PTI calculation with the reaction to diketene having 31 points and the reaction to the butadione 28.

The calculation of the butadione reaction curve proceeded without any difficulties giving a corrected free energy of reaction of $\Delta A_{CM} = -4.5$ (−3.0) kcal/mol and a free energy barrier of $\Delta A^{\ddagger}_{CM} = 26.4$ (29.9) kcal/mol at a value of the reaction coordinate of approximately 3.9 (3.9) bohr (2.06 Å). The values in parentheses are the corresponding numbers derived from frequency calculations.

The PTI calculation of the reaction to form diketene was not so straightforward, however. The transition state of this reaction has a mostly formed C−C bond but with a largely unformed C−O bond and has a geometry with C_1 symmetry rather than the C_s symmetry of the product molecule[71] (see Figure 6). CISD calculations put the length of the C−C bond at 3.33 bohr (1.76 Å), the C−O bond distance at 5.05 bohr (2.67 Å), and the O−C−C−C dihedral angle at −56°.[71] The trajectories obtained from our simulations show that at the transition state and for somewhat larger values of the reaction coordinate the mode corresponding to changes in this dihedral angle is very soft allowing large amplitude vibrations: so large, that in some cases the dihedral angle became close to 180° causing the simulation to fall into the minimum corresponding to the cyclobutadione product. In other words, there is a bifurcation in the minimum energy path with one branch leading to each of the known products. Motion of the simulation along one part of the bifurcation is prevented by the constraint required for thermodynamic integration. Motion in the other direction is not restricted, however, and can lead the simulation to wander a long way away from the desired reaction path. This problem can be particularly problematic if, as is the case here, the

potential energy surface is flat and perhaps decreasing in energy in this direction. Unfortunately in this case, the value of the constraint where the bifurcation occurs (~4.15 bohr or 2.20 Å) corresponds to a butadione structure near its local minimum.

The ensemble average forces at the points in the PTI calculation that wandered into the butadione minimum were unreasonably high causing the calculated free energy of reaction to be significantly in error. The alternative STI method was attempted but also fell into the alternative minimum, resulting in a completely unreasonable free energy curve as the continual small stepping of the constraint tore the molecule apart.

The simple-minded solution to the problem was to ignore any contributions to ensemble forces once a simulation had entered the cyclopentadiene minimum. This resulted in three of the PTI points at reaction coordinates of 3.75 (25 000), 3.875 (21 000) and 4.0 (7000) bohr having less than the desired number of 30 000 time steps. The number of time steps in the simulations before the trajectory wandered into the undesired minimum are listed in parentheses after the reaction coordinate values. Calculations with the reaction coordinate chosen to be between 4.1 and 4.2 bohr gave less than 5000 usable time steps and were discarded. Integrating the average forces obtained from the acceptable parts of the trajectories resulted in a corrected reaction free energy to diketene $\Delta A_{CM} = -5.5$ kcal/mol and a corrected barrier at 3.69 bohr (1.95 Å) of $\Delta A^{\ddagger}_{CM} = 31.5$ kcal/mol. The equivalent values from frequency calculations are −5.9 and 34.7 kcal/mol. The good agreement between the dynamic and static results, particularly for the overall reaction energy for which frequency analyses should perform very well, suggests that the simple-minded approach used here to deal with the bifurcation may work well.

Rather than applying the rather ad hoc approach described here, the formation of the undesired product could be prevented by the application of an artificial repulsive potential. This method has the advantage that longer and better equilibrated simulations could be performed.

These calculations predict that the free energy barrier to the formation of diketene is in fact rather higher than the barrier to formation of 1,3-butadione and that the diketene is the observed product because of thermodynamic control. This is contrary to the conclusions drawn in previous publications[71,72] where the barrier to the formation of diketene is lower. Only the enthalpy barrier was discussed in these papers. The internal energy barriers in the present calculations, $\Delta U^{\ddagger}$, are calculated to be 16.4 and 21.2 kcal/mol for the butadione and diketene reaction, respectively. The difference between $\Delta U^{\ddagger}$ and $\Delta A^{\ddagger}_{CM}$ is close to 10 kcal/mol for both reactions, so entropic effects do not appear to favor one path over the other. It therefore might be expected that the conflicting predictions are due to the differing quality in electronic structure methods used. The CCSD(T) numbers from ref 72 are likely to be the most reliable though the basis set used in this work was relatively small.

Concluding Remarks

We now address several general points concerning all systems studied. The temperatures at each point of the PTI simulations was monitored, with averages taken over the last half of the time steps taken. The mean temperatures were within the range of 300 ± 15 K. Assuming that internal energy and entropy changes are not significantly affected within this temperature range, the definition of $\Delta A = \Delta U - T\Delta S$ can give a simple relative error estimate of the entropic contribution to the free energy as follows: error = 15 K/300 K = 5%. This temperature error is likely within ±0.5 kcal/mol for the systems studied.

The convergence analysis of the PTI method indicates that, while the error does decrease with the increase of the times steps used at each point, any number of time steps over 10 000 per point will usually give convergence to ±1 kcal/mol as long as the reaction coordinate chosen is a good one. More time steps per point are needed if the reaction coordinate is less than ideal as was the case for the butadiene + ethene and the cyclopropanation reactions. Because the integration procedure used for the PTI method involves a local quadratic approximation (Simpson's rule), the positions of the PTI points will give the most accurate results when they are dense enough to make that assumption valid. It has been our experience that around the transition state, a spacing of 0.125 bohr (approximately 0.07 Å) is required, whereas at long reagent separation 0.5 bohr (0.26 Å) is sufficient. Once this sufficient number of points has been reached or surpassed, we have estimated the numerical error of integration to be within ±0.5 kcal/mol by adding and removing mean force points at various positions along the reaction coordinate. In terms of computational expense, once equilibration has been performed, the PTI method will take approximately 300 000 to 1 500 000 times steps to provide accurate results. In contrast, the slow-growth method appears to require at least a 400 000 time step simulation, in both directions; thus, at least 800 000 time steps and possibly up to 1 600 000 time steps are required. Overall, the PTI method may require less computational time that the STI scheme. Furthermore, it has the added advantages that many PTI points may be run concurrently and a given PTI calculation may easily be improved.[10]

The net translation and rotation of the system was removed in all AIMD calculations. It has not been established exactly what the effect of this is on the rotation of the individual reactants, though it was assumed here that they can rotate freely if their interaction with each other is negligible. Given the good agreement between the ΔA_{CM} and $\Delta A_{QM'}$ values for each of the free energies of reaction, it seems that this assumption is reasonable. However, it should be kept in mind that the rotation of the separated reactants is not completely free. For example, the rotation of two molecules in the same direction about the axis passing through the center of mass of each is not allowed if the rotation of the total system is constrained. Essentially, the removal of the system's angular momentum about its center of mass will impose a constraint, of unknown form, on the individual rotations of the reagents about their molecular centers of mass that may affect the rotational entropy of the system.

It is well-known that for small systems the standard Nosé−Hoover thermostat does not produce ergodic trajectories.[17,48,75,76] At the inception of the work described in this paper, it had been expected that the improved thermostat suggested by Blöchl[19] would not provide similar problems. Clearly, given the results described here, although the improved thermostat is superior to the standard version, it is still not satisfactory for the present purposes. The obvious next step is to try the Nosé−Hoover chain thermostat,[48] an alternative improvement upon the basic formulation. Rather than repeat the numerous calculations already discussed with a third thermostat, three test calculations were performed with a Nosé−Hoover chain thermostat of length six. The systems chosen were that for which the Blöchl-improved thermostat performed the most poorly (the syn Diels−Alder reaction of ethene and amino-cyclopentadiene) and two other randomly chosen reactions (the Diels−Alder reaction of ethene and butadiene and the dimerization of ketene). All test calculations were at a value of the reaction coordinate of 9.449 bohr (5 Å) where the reactant molecules should be free to rotate.

Each calculation was run for at least 4 ps and the energy of each rotational mode analyzed by the procedure described during the discussion of the Diels−Alder results. With one exception, the rotational modes all had average energies of about 0.06 kcal/mol, somewhat less than the 0.3 kcal/mol required at 300 K. The exception was one rotational mode of ethene in the syn Diels−Alder reaction, which had an average energy of more than 0.5 kcal/mol. Closer examination found that this mode had been highly excited during the warm-up phase of the simulation but that almost all of the energy in this mode had gone after the simulation had run for 2 ps. Extending the simulation to 6 ps gave no noticeable increase in the energy of this mode, and it therefore is expected that after a long enough simulation time the average energy in this mode would be about 0.05 kcal/mol.

The performance of the Nosé−Hoover chain thermostat was further tested by calculation of the syn Diels−Alder reaction of ethene and amino-cyclopentadiene at 9.449 bohr with several characteristic frequencies of the thermostat.The total rotational kinetic energy of the individual molecules did vary as a function of this frequency but was never greater than 50% of $^3/_2$RT and generally did not distribute the rotational energy evenly among the three rotational modes.

It appears that the Nosé−Hoover chain thermostat, though superior to the conventional Nosé thermostat of the improved version of ref 19, is also unable to maintain sufficient energy in the rotational modes of two isolated molecules.

The results and discussion presented here have established several key findings in the theory and implementation of AIMD with the goal of calculating free energy profiles along entire reaction curves. Although simple a priori reaction coordinates were used, the results should be applicable to more complicated IRC-type reaction coordinates.

The phase-space sampling methods slow-growth (STI) and point-wise (PTI) thermodynamic integration were applied in a variety of illustrative bimolecular reactions. Helmholtz free energy changes were calculated by thermodynamic integration. The results obtained in studying the same system under both sampling methods show that they give very similar free energy profiles. The PTI method may be used successfully in cases where as STI calculation will wander off the desired reaction path.

The Nosé−Hoover or the Andersen thermostat was used to control the nuclear temperatures (kinetic energies), and in many cases their performances were compared. The Nosé thermostat was found to poorly equilibrate systems leading to modes with very little energy (in particular rotational modes) and to an underestimated and typically incorrect entropic contribution to the free energy change. The Andersen thermostat did equilibrate the rotational modes as shown by an analysis of the energy in the relevant mode. Specifically, when applied to the PTI method the Andersen thermostat afforded results with significant entropic effects and with free energy changes and barriers in good agreement with the results of frequency analyses.

In a broad sense, the results presented here contribute to the validation of the usage of AIMD (specifically Car−Parrinello theory) in the modeling of chemical reactions and the calculation of free energies along the reaction curve.

Acknowledgment. We thank Dr. Paul Fleurat-Lessard, Dr. Artur Michalak, and Dr. Hans-Martin Senn for helpful discussions. This work has been supported by the National Sciences and Engineering Research Council of Canada (NSERC). Calculations were performed in part on the MACI Alpha cluster located at the University of Calgary. T.Z. thanks the Canadian government for a Canada Research Chair.

References and Notes

(1) Mugnai, M.; Cardini, G.; Schettino, V. *J. Phys. Chem. A* **2003**, *107*, 2540.
(2) Kuhn, B.; Kollman, P. A. *J. Am. Chem. Soc.* **2000**, *122*, 6299.
(3) Carloni, P.; Rothlisberger, U.; Parrinello, M. *Acc. Chem. Res.* **2002**, *35*, 455.
(4) Mundy, C. J.; Colvin, M. E.; Quong, A. A. *J. Phys. Chem. A* **2002**, *106*, 10063.
(5) Tse, J. S. *Annu. Rev. Phys. Chem.* **2002**, *53*, 249.
(6) Michalak, A.; Ziegler, T. *J. Phys. Chem. A* **2001**, *105*, 4333.
(7) Marx, D.; Hutter, J. Ab Initio Molecular Dynamics: Theory and Implementation. In *Modern Methods and Algorithms of Quantum Chemistry*; Grotendorst, J., Ed.; John von Neumann Institute of Computing: Jülich, 2000; p 301.
(8) Baveridge, D. L.; DiCapua, F. M. *Annu. Rev. Biophys. Chem.* **1989**, *18*, 431.
(9) Ammal, S. C.; Yamataka, H.; Aida, M.; Dupuis, M. *Science* **2003**, *299*, 1555.
(10) Straatsma, T. P. Free Energy by Molecular Simulation. In *Reviews in Computational Chemistry*; Lipkowitz, K. B., Boyd, D. B., Eds.; VCH Publishers: New York, 1996; Vol. 9, p 81.
(11) Zwanzig, R. W. *J. Chem. Phys.* **1954**, *22*, 1420.
(12) Carter, E. A.; Ciccotti, G.; Hynes, J. T.; Kapral, R. *Chem. Phys. Lett.* **1989**, *156*, 472.
(13) Paci, E.; Ciccotti, G.; Ferrario, M.; Kapral, R. *Chem. Phys. Lett.* **1991**, *176*, 581.
(14) den Otter, W. K.; Briels, W. J. *J. Chem. Phys.* **1998**, *109*, 4139.
(15) Straatsma, T. P.; McCammon, J. A. *J. Chem. Phys.* **1991**, *95*, 1175.
(16) Nosé, S. *Mol. Phys.* **1986**, *57*, 187.
(17) Hoover, W. G. *Phys. Rev. A: At., Mol., Opt. Phys.* **1985**, *31*, 1695.
(18) Blöchl, P. E.; Parrinello, M. *Phys. Rev. B: Solid State* **1992**, *45*, 9413.
(19) Blöchl, P. E. *Phys. Rev. B: Solid State* **2002**, *65*, 104303.
(20) Andersen, H. C. *J. Chem. Phys.* **1980**, *72*, 2384.
(21) Car, R.; Parrinello, M. *Phys. Rev. Lett.* **1985**, *55*, 2471.
(22) Woo, T. K. Towards More Realistic Molecular Modeling of Catalysis with Density Functional Theory: Combined QM/MM and ab Initio Molecular Dynamics Methods. Ph.D. Thesis, University of Calgary, 1998.
(23) Fukui, K. *Acc. Chem. Res.* **1981**, *14*, 363.
(24) Blöchl, P. E. *Phys. Rev. B: Solid State* **1994**, *50*, 17953.
(25) Blöchl, P. E. *J. Phys. Chem.* **1995**, *99*, 7422.
(26) Perdew, J. P.; Wang, Y. *Phys. Rev. B: Solid State* **1992**, *45*, 13244.
(27) Becke, A. *Phys. Rev. A: At., Mol., Opt. Phys.* **1988**, *38*, 3098.
(28) Perdew, J. P. *Phys. Rev. B: Solid State* **1986**, *33*, 8822.
(29) Ryckaert, J.-P.; Cicotti, G.; Berensden, H. J. C. *J. Comput. Phys.* **1977**, *23*, 327.
(30) Te Velde, G.; Bickelhaupt, F. M.; Baerends, E. J.; Fonseca Guerra, C.; Van Gisbergen, S. J. A.; Snijders, J. G.; Ziegler, T. *J. Comput. Chem.* **2001**, *22*, 931.
(31) Guerra, C. F.; Snijders, J. G.; Te Velde, G.; Baerends, E. J. *Theor. Chem. Acc.* **1998**, *99*, 391.
(32) *ADF*, 2002.03 ed; SCM, Theoretical Chemistry, Vrije Universiteit: Amsterdam, The Netherlands, 2002.
(33) Vosko, S. H.; Wilk, L.; Nusair, M. *Can. J. Phys.* **1980**, *58*, 1200.
(34) McQuarrie, D. A. *Statistical Thermodynamics*; Harper and Row: New York, 1973.
(35) Anane, H.; Boutalib, A.; Tomás, F. *J. Phys. Chem. A* **1997**, *101*, 7879.
(36) Greiner, W.; Neise, L.; Stöcker, H. *Thermodynamics and Statistical Mechanics*; Springer-Verlag: New York, 1995.
(37) Borden, W. T.; Loncharich, R.; Houk, K. N. *Annu. Rev. Phys. Chem.* **1988**, *39*, 213.
(38) Houk, K. N.; Beno, B. R.; Nendel, M.; Black, K.; Yoo, H. Y.; Wilsey, S.; Lee, J. K. *J. Mol. Struct. (THEOCHEM)* **1997**, *398*, 169.
(39) Houk, K. N.; Lin, Y. T.; Brown, F. K. *J. Am. Chem. Soc.* **1988**, *108*, 554.
(40) Li, Y.; Houk, K. N. *J. Am. Chem. Soc.* **1993**, *115*, 7478.
(41) Dewar, M. J. S.; Jie, C. *Acc. Chem. Res.* **1992**, *25*, 537.
(42) Karadakov, P. B. *J. Am. Chem. Soc.* **1998**, *120*, 3975.
(43) Sakai, S. *J. Phys. Chem. A* **2000**, *104*, 922.
(44) Xidos, J. D.; Poirier, R. A.; Pye, C. C.; Burnell, D. J. *J. Org. Chem.* **1998**, *63*, 105.
(45) Tachibana, A.; Fukui, K. *Theor. Chem. Acta* **1980**, *57*, 81.
(46) Goldstein, H. *Classical Mechanics*, 2nd ed.; Addison-Wesley: Reading, MA, 1980.
(47) Samuelson, S.; Martyna, G. J. *J. Phys. Chem. B* **1999**, *103*, 1752.
(48) Martyna, G. J.; Tuckerman, M.; Klein, M. L. *J. Chem. Phys.* **1992**, *97*, 2635.

(49) Tobias, D. J.; Martyna, G. J.; Klein, M. L. *J. Phys. Chem.* **1993**, *97*, 9.
(50) Martyna, G. J.; Tuckerman, M.; Tobias, D. J.; Klein, M. L. *Mol. Phys.* **1996**, *87*, 1117.
(51) Jang, S.; Pak, Y.; Shin, S. *J. Chem. Phys.* **2002**, *116*, 4782.
(52) Macaulay, J. B.; Fallis, A. G. *J. Am. Chem. Soc.* **1990**, *112*, 2.
(53) Poirier, R. A.; Pye, C. C.; Xidos, J. D.; Burnell, D. J. *J. Org. Chem.* **1995**, *60*, 2328.
(54) Ishida, M.; Kakita, S.; Inagaki, S. *Chem. Lett.* **1995**, 469.
(55) Kahn, S. D.; Hehre, W. J. *J. Am. Chem. Soc.* **1987**, *109*, 663.
(56) Anh, N. T. *Tetrahedron* **1973**, *29*, 3227.
(57) Brown, F. K.; Houk, K. N.; Burnell, D. J.; Valenta, Z. *J. Org. Chem.* **1987**, *52*, 3050.
(58) Williamson, K. L.; Hsu, Y.-F. L. *J. Am. Chem. Soc.* **1971**, *92*, 7385.
(59) Rondan, N. G.; Houk, K. N.; Moss, R. A. *J. Am. Chem. Soc.* **1980**, *102*, 1770.
(60) Wong, P. C.; Griller, D.; Scaiano, J. L. *Chem. Phys. Lett.* **1981**, *103*, 2423.
(61) Turro, N. J.; Lehr, G. F.; Butcher, J. A.; Moss, R. A.; Guo, W. *J. Am. Chem. Soc.* **1982**, *104*, 1754.
(62) Moss, R. A.; Perez, L. A.; Turro, N. J.; Gould, I. R.; Hacker, N. P. *Tetrahedron Lett.* **1983**, *24*, 685.
(63) Houk, K. N.; Rondan, N. G.; Mareda, J. *J. Am. Chem. Soc.* **1984**, *106*, 4291.
(64) Blake, J. F.; Wierschke, S. G.; Jorgensen, W. L. *J. Am. Chem. Soc.* **1989**, *111*, 1119.
(65) Krogh-Jespersen, K.; Yan, S.; Moss, R. A. *J. Am. Chem. Soc.* **1999**, *121*, 6269.
(66) Miller, B. *Advanced Organic Chemistry*; Prentice-Hall: New Jersey, 1998.
(67) Keating, A. E. *J. Am. Chem. Soc.* **1999**, *121*, 3933.
(68) Tidwell, T. T. *Ketenes*; Wiley: New York, 1995.
(69) Tenud, L.; Weilmann, M.; Dallwigk, E. *Helv. Chim. Acta* **1977**, *60*, 975.
(70) Fu, X. Y.; Decai, F.; Yanbo, D. *J. Mol. Struct.* **1988**, *167*, 349.
(71) Seidl, E. T.; Schaefer, H. F. *J. Am. Chem. Soc.* **1991**, *113*, 5195.
(72) Salzner, U.; Bachrach, S. M. *J. Am. Chem. Soc.* **1994**, *116*, 6850.
(73) De Raedt, B.; Sprik, M.; Klein, M. L. *J. Chem. Phys.* **1984**, *80*, 5719.
(74) Wilsey, S.; Houk, K. N.; Zewail, A. H. *J. Am. Chem. Soc.* **1999**, *121*, 5772.
(75) Toxvaerd, S.; Olsen, O. H. *Ber. Bunsen-Ges. Phys. Chem.* **1990**, *94*, 274.
(76) Posch, H. A.; Hoover, W. G.; Vesely, F. J. *Phys. Rev. A: At., Mol., Opt. Phys.* **1986**, *33*, 4253.
(77) Kierstead, W. P.; Wilson, K. R.; Hynes, J. T. *J. Chem. Phys.* **1991**, *95*, 5256.
(78) Frank, K. I.; Parinello, M.; Klamt A. *J. Phys. Chem. A* **1998**, *102*, 3614.
(79) Sprik, M. *Chem. Phys.* **2000**, *258*, 139.
(80) Pagliai, M.; Raugei, S.; Cardini, G.; Schettino, V. *J. Chem. Phys.* **2003**, *119*, 9063.
(81) Wang, I. S. Y.; Karplus, M. *J. Am. Chem. Soc.* **1973**, *95*, 8160.
(82) Ishikawa, Y.; Gong, Y; Weiner, B. *Phys. Chem. Chem. Phys.* **2000**, *2*, 869.
(83) Bernhardt, E.; Willner, A.; Kornarth, A.; Breidung, J.; Bühl, M.; Jonas, V.; Thiel, W. *J. Phys. Chem. A* **2003**, *107*, 859.
(84) Hase, W. L.; Song, K. H.; Gordon, M. S. *Comput. Sci. Eng.* **2003**, *5*, 36.